Mem. S.A.It. Suppl. Vol. 1, 155

Memorie della
Supplementi

Propagation of extragalactic jets in stratified media

C. Zanni[1], S. Massaglia[1], G. Bodo[2], P. Rossi[2], A. Capetti[2], and A. Ferrari[1]

[1] Dipartimento di Fisica Generale dell'Università, Via Pietro Giuria 1, I - 10125 Torino
email: massaglia@ph.unito.it
[2] INAF – Osservatorio Astronomico di Torino, Strada dell'Osservatorio 20, I-10025 Pino Torinese
email: bodo@to.astro.it

Abstract. We perform numerical hydrodynamic simulations in order to study the interaction between a supersonic jet and a medium stratified by the gravitational potential. Several observations of extragalactic radio sources show strong evidences of interaction between the radio lobes and the external atmosphere: on one hand X-ray observations show several cases in which the radio lobes displace the surrounding cluster gas; on the other hand radio images show some peculiar lobe morphologies that can be explained taking into account the interaction of the jet with an anisotropic ambient medium. In order to model different environments we consider stratifications with different symmetries: spherical, elliptical and triaxial. Thanks to the simulations with a spherically stratified environment we obtain informations on the X-ray emission properties of the ambient perturbed by the jet; with the simulations with an anisotropic stratification we can study the effects of the ambient medium on the morphology of the radio lobes.

Key words. Hydrodynamics – Galaxies: jets – Galaxies: active

1. Introduction

The general structure of the interaction between a low density supersonic jet and the ambient medium is well known since the first simulations of Norman et al. (1982): the flowing jet matter, slowed down by one or more terminal shocks, inflates a cocoon that compresses and drives shocks in the surrounding external medium. The compressed ambient material forms a shell surrounding the cocoon: the boundary between the shell and the cocoon is marked by a contact discontinuity, while the boundary between the shell and the undisturbed external medium is marked by a shock. This basic framework was studied in great detail by Massaglia et al. (1996) who performed a numerical analysis of the propagation of supersonic jets in a uniform ambient medium and showed how the cocoon morphology depends on the Mach number and density ratio of the jet to the exteriors. Recently Krause (2002) simulated the propagation of axisymmetric very light jets and showed

Send offprint requests to: S. Massaglia

how the morphology of the simulated cocoons can be compared to the observed radio sources. Clarke, Harris & Carilli (1997) carried out calculations of the jet propagation in a spherical symmetric King atmosphere obtaining simulated X-ray images to compare with ROSAT data on Cygnus A who showed deficits of X-ray emission in the cluster gas spatially coincident with the radio lobes (Carilli, Perley & Harris 1994). A similar scenario is depicted by numerical simulations of Rizza et al. (2000) who showed the interaction and disruption of a jet inside a cooling flow cluster. More recently Reynolds et al. (2001), studying the propagation of a jet inside a β-model cluster atmosphere, have shown the dynamical evolution of the cocoon that start being strongly overpressured, but, during its evolution, the pressure decreases, and it becomes essentially in pressure equilibrium with the ambient. Reynolds et al. (2002) extended the study of the evolution of the cocoon inside a stratified medium to the phase in which the jet activity has ceased and investigated the evolution of the relics of the cocoon.

In this paper we analyze in detail the interaction between an underdense supersonic jet with a stratified ambient medium by mean of numerical simulations in two and three dimensions. We take into account various atmospheres with different symmetries: spherical, elliptical and triaxial. The simulations in a spherically stratified ambient medium confirm the results by Reynolds, Heinz & Begelman (2001) on the two distinct regimes of interaction, with strong or weak shocks but we are able to determine how this transition occurs, depending on the jet parameters. We also relate the different stages of evolution of a cocoon inside a stratified medium with the observed X-ray emission of the ambient gas perturbed by the jet. In order to better understand some peculiar features in the radio emission in extended radio sources, we simulate also elliptical and triaxial stratifications and we study their effects on the cocoon morphology.

In Section 2 we present the results of the simulations of the propagation of a jet inside a spherically stratified atmosphere. We study the dynamical and morphological evolution of the cocoon and the X-ray emission properties of the ambient medium perturbed by the jet. In Section 3 we present the results of the simulations of the interaction of a jet with an anisotropically stratified medium. We consider 2D simulations with an elliptical stratification with cylindrical symmetry and 3D simulations with a triaxial stratification.

2. Spherical stratification

2.1. Astrophysical scenario

X-ray observations of extragalactic radio sources revealed strong evidences of interaction between the radio emitting plasma and the X-ray emitting gas in the ambient medium of groups and clusters of galaxies. The observations of Cygnus A with the ROSAT HRI (Carilli, Perley & Harris 1994) and with the Chandra X-ray Observatory (Smith et al. 2002) showed regions devoid of of X-ray emission coincident with the radio lobes. Deficits of X-ray emission spatially coincident with the lobes of the radio galaxies have been observed in the Perseus cluster (Böhringer et al. 1993, Fabian et al. 2000), in the Hydra A cluster (McNamara et al. 2000, Nulsen et al. 2002) and in Abell 2052 (Blanton et al. 2001). Also rims of enhanced emission have been observed surrounding the cavities but in many cases (Perseus A, Hydra A, A 2052) they are cooler than the surrounding ambient medium.

2.2. Numerical simulations

We solved numerically the hydrodynamic equations for a supersonic jet, in cylindrical (axial) symmetry in the coordinates (r, z) continuously injected into a gravitationally stratified (but not self-gravitating) medium. The basic equations have been solved numerically employing

a PPM (Piecewise Parabolic Method) hydrocode (Woodward & Colella 1984). The integration domain has a size $r_{\rm domain} \times z_{\rm domain}$ where $r_{\rm domain} = z_{\rm domain} = 2.6a$, where a is the core radius, defined below, and has been divided in 1024×1024 grid points. The axis of the jet is along the left boundary of the domain ($r = 0$), where we have imposed symmetric boundary conditions for p, ρ, v_z and antisymmetric conditions for v_r. Reflective boundary conditions are also imposed on the boundary of injection of the jet ($z = 0$) outside its radius in order to reproduce a bipolar flow and to avoid spurious inflow effects. Free outflow is set on the remaining boundaries by imposing a null gradient for each variable ($d/dr = 0$).

The undisturbed ambient medium is assumed stratified in a spherically symmetric gravitational well, according to a classical isothermal King model:

$$\rho_{\rm ext}(R) = \frac{\rho(0)}{\left[1 + (R/a)^2\right]^{3\beta/2}} \ , \qquad (1)$$

with $R = \sqrt{r^2 + z^2}$ and $\beta = 0.5$. The resulting pressure stratification is kept in equilibrium by an appropriated external gravitational potential. A (cylindrical) jet with a radius $r_{\rm j} = a/20$ is injected from the bottom boundary of the integration domain, in pressure balance with the ambient. Measuring lengths in units of the core radius a, velocities in units of the adiabatic sound speed $c_{\rm se}$ in the undisturbed external medium and the density in units of the ambient central density $\rho(0)$, our main parameters are the Mach number $M \equiv v_{\rm j}/c_{\rm se}$ and the density ratio $\nu = \rho_{\rm j}/\rho(0)$. In this Paper we consider only three significant cases, that is three jets with $M = 60$ and $\nu = 0.1$, $\nu = 0.01$ and $\nu = 0.001$ respectively.

2.3. The cocoon dynamics

In Fig. 1 we show the density distribution for the simulated cases: each row refer to a different density ratio ($\nu = 0.1, 0.01, 0.001$ from top to bottom) and each column is for different times corresponding to cocoon lengths $1, 1.5, 2$ respectively. The numerical simulations show that the expanding cocoon drives a shock in the ambient medium, which is then compressed and heated. The strength of the shock driven by the cocoon depends essentially on the ratio between the mean cocoon pressure and the decreasing pressure of the ambient medium. In Fig. 2 we plot the behavior of $P_{\rm c}$ (solid curve) and P^* (dashed curve) against the cocoon length for the $M = 60$ cases, where $P_{\rm c}$ is the average cocoon pressure and P^* is the external pressure averaged over the cocoon volume.

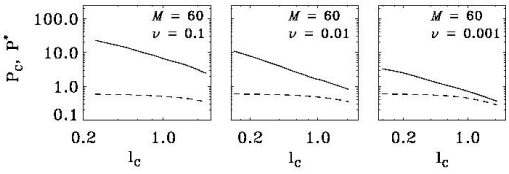

Fig. 2. Plot of the pressure vs cocoon length. Columns refer to the different ν values of the $M = 60$ cases. The solid line shows the evolution of the average cocoon pressure with time in the different cases. The dashed one represents the external pressure averaged on the cocoon volume

We see that the cocoon pressure is much greater than the ambient one for the case $\nu = 0.1$; the $\nu = 0.01$ case shows a transition from a strongly to a weakly overpressured cocoon while in the $\nu = 0.001$ case the cocoon is always weakly overpressured. This tells us that the $\nu = 0.1$ cocoon is driving a strong shock in the ambient medium during the whole simulated time while in the $\nu = 0.01$ the bow shock becomes weaker during the evolution of the cocoon; in the $\nu = 0.001$ case the shock is always weak and the cocoon tends to expand at the sound speed. We see in Fig. 1 that the different regimes of expansion correspond to different morphologies of the cocoon and of the shell of compressed am-

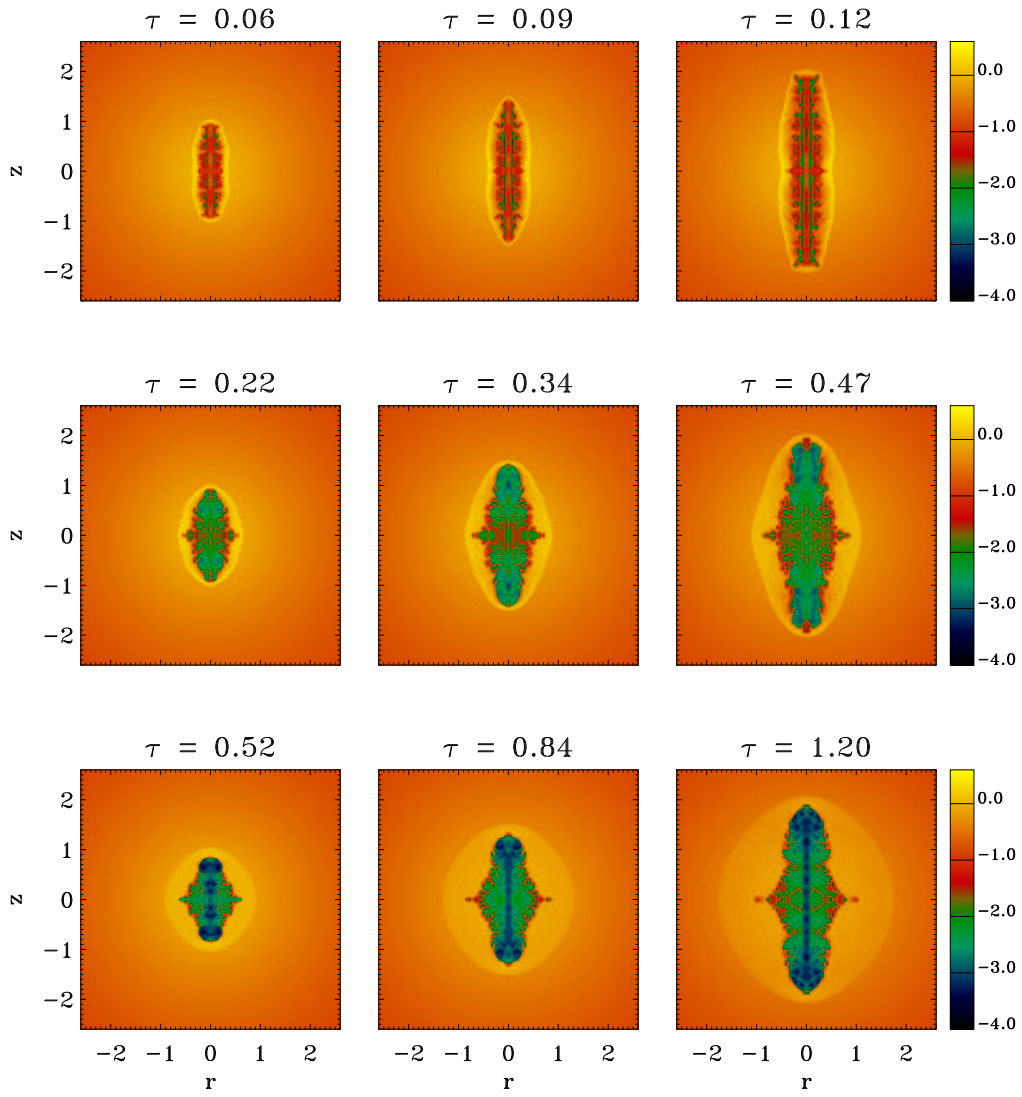

Fig. 1. Density maps for the $M = 60$ cases. The scale is logarithmic. The rows refer from top to bottom to the $\nu = 0.1, 0.01, 0.001$ cases respectively. In the columns density maps are shown at times corresponding to a cocoon length $l_c \sim 1, 1.5$ and 2 core radii. The densities are given in unity of the central density of the unperturbed atmosphere

bient material that surrounds it. In particular we see that the width of the shell increases going from the high to the low ν cases. Moreover we can see that the shell tends to widen only in the cases in which the bow shock becomes weaker during the evolution of the cocoon. In agreement with the results presented by Reynolds, Heinz & Begelman (2001), we find then two distinct and subsequent regimes of interaction between the cocoon and the external medium. In the first phase of evolution, the overpressured cocoon drives a strong shock in the ambient medium, forming a thin, hot and

compressed shell of shocked material, in the second phase the shock becomes very weak and the shell widens, decreasing its density and temperature.

2.4. X-ray signature: shell and cavity

The simulations show us that the cocoon, which is formed by the expanded jet material, forms a cavity with very low density and high temperature while the external material is compressed and heated by the shock driven by the expanding cocoon. In principle, we then expect two main features in the X-ray properties of the region of interaction between a jet and the ambient medium:

- a region of depressed emission coincident with the cocoon;
- a shell of enhanced emission.

In Fig. 3 we show in the first two columns simulated X-ray flux distribution for the cases described in the table. The figures are symmetrical with respect to the r and z axes. The emissivity per frequency unit is computed with a Raymond-Smith thermal spectrum code from the electron density and temperature distribution obtained in our calculation. The emissivity $\epsilon = n^2\Lambda(T)$ is then integrated in the $0.1 - 4$ KeV band. The flux distribution is calculated integrating the optically thin emissivity along the line of sight that is assumed perpendicular to the jet axis. We consider an isothermal ambient medium with a temperature $T = 2.3$ KeV and a central electron density $n_0 = 0.01\,\mathrm{cm}^{-3}$. In Fig 3 we show the results for the three cases, each row refer to a different value of the density ratio and more precisely the top row is for $\nu = 0.1$, the middle row is for $\nu = 0.01$ and the bottom row is for $\nu = 0.001$. The first two panels in a row are for a different time and we have chosen the times in order to have lengths respectively of 1 and 2 core radii. A more quantitative view of these results can be obtained presenting cuts of these figures along selected directions. In particular in Fig. 3 in the third and fourth column we show longitudinal cuts of the images along the jet axis. The dashed curves in all the figures represent the emission from the undisturbed atmosphere.

These panels show a sequence of morphologies starting from cases in which a cavity is not present going to cases in which the cavity is the dominant feature of the image. In particular, we see that the brightness depression is absent for $\nu = 0.1$, starts to be present for $\nu = 0.01$ during its evolution and is very evident during the whole evolution for $\nu = 0.001$.

The presence or absence of the brightness depression depends on the thickness of the shell. In fact, the line of sight that goes through the cocoon region with very low emissivity crosses also the shell of enhanced emissivity, and the observed flux is higher or lower than the undisturbed profile depending on the interplay between the two effects. If the shell is narrow, as a consequence of mass conservation, it will have a high density, the emissivity will be greatly enhanced and will overcome the decrease in the cocoon giving an observed brightness higher than the undisturbed profile. As discussed in the previous section the relative thickness of the shell is allowed to increase only if the cocoon is in a weakly overpressured regime while it remains compressed and constant in the strongly overpressured phase. As we expect from the brief discussion on the cocoon dynamics the $\nu = 0.1$ case shows no cavity and a strongly enhanced shell of emission, while the other two cases begin to form a cavity only when the cocoon pressure becomes comparable to the external one.

Then the regimes of expansion correspond to different X-ray morphologies: an overpressured cocoon shows no deficit of emission and a hot and compressed shell of enhanced emission marking the shock driven by the cocoon; a weakly overpressured cocoon shows a deficit of emission surrounded by an expanded shell much less visible than in the overpressured case. Then the simulations tell us that the cocoons that form the radio lobes must be

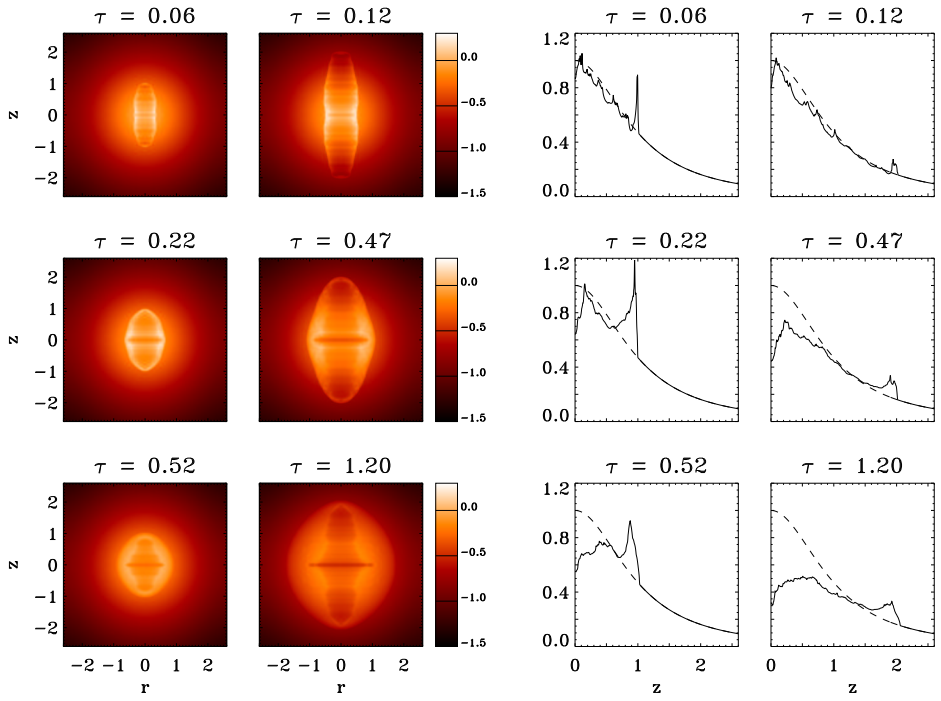

Fig. 3. Simulated X-ray fluxes in the $0.1 - 4$ KeV band for the simulated cases. The rows refer from top to bottom to the $\nu = 0.1, 0.01, 0.001$ cases respectively. In the first two columns on the left the X-ray images are shown in logarithmic scale at times corresponding to cocoon lengths of $l_c \sim 1$ and 2 core radii. In the two columns on the right longitudinal cuts along to the jet axis corresponding to the images on the left are plotted with a solid line. The dashed line represents the emission from the undisturbed atmosphere. The fluxes are given in unity of the central flux of the unperturbed atmosphere

in a weakly overpressured regime in order to form a cavity, driving a weak shock in the ambient medium: this fact is in agreement also with the observations of cool rims surrounding some of the X-ray cavities (Perseus A, Hydra A, A 2052) that rule out the possibility of strong shocks driven by the expanding cocoon.

3. Anisotropic stratification

3.1. Astrophysical scenario

A significant fraction of extended radio sources presents a peculiar X-shaped radio morphology: in addition to the classical double lobed structure, radio emission is also observed along a second axis of symmetry in the form of diffuse wings or tails. In Capetti et al. (2002) we have shown that the orientation of the wings shows a striking connection with the structure of the host galaxy, as they are preferentially aligned with its minor axis. Moreover we also have shown that X-shaped radio sources occur exclusively in galaxies of high ellipticity. In Fig. 4 we show two sources taken from the sample of Capetti et al. (2002) to give an idea of the morphology we are considering. In each panel the host galaxy shape is superposed.

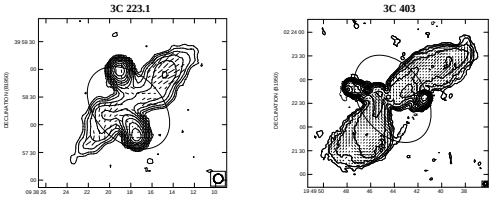

Fig. 4. Superposition of the host galaxy shape (not in scale) onto the radio maps for two X-shaped radio sources.

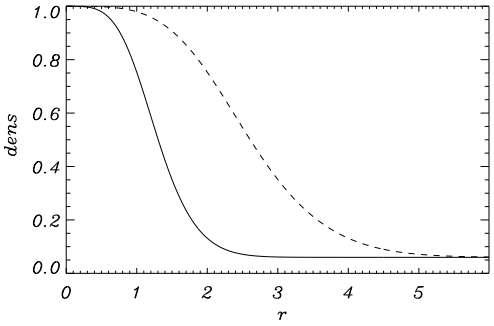

Fig. 5. Equilibrium density profile of the adopted external gas distribution. The gas has an ellipsoidal shape and here we present the density profiles along the major (dashed line) and minor (solid line) axis.

3.2. 2D Simulations

The results shown in the previous section suggest that the distribution of the external gas plays an important role in the evolution of the morphology of the radio lobes. In order to consider the effects of anisotropies in the stratification of the ambient medium on the morphology of the cocoons we performed numerical simulations of the propagation of a jet in a stratified medium with an elliptical symmetry. The adopted external gas distribution has an elliptical shape and, in Fig, 5 we represent the the density profiles along the major and minor axis. The width $r_{\rm c}$ of the central plateau along the major axis is chosen as our unit of length. The gas is isothermal and is kept in equilibrium by an appropriated gravitational potential. The integration is performed in cylindrical geometry, the computational domain extends up to $6r_{\rm c}$ in the r direction and up to $9r_{\rm c}$ in the z direction and is covered by 704×1024 points. The boundary conditions are the same as in the cases with the spherical stratification. The jet has a radius $r_{\rm j} = 0.1r_{\rm c}$, a Mach number $M = 60$ and a density 3×10^{-3} times the central value in the external medium. In order the better understand the role played by the external stratification in shaping the morphology of the cocoon, we performed two simulations, with the jet oriented along and perpendicularly to the stratification major axis.

In Fig 6 we show density images representing the evolution of the radio source in the anisotropically stratified medium. The top panels refer to the case when the jet is oriented parallel to the major axis of the distribution, while the lower panels to the case when the jet is oriented parallel to the minor one.

In the very initial stages, when the radio source size is smaller than the central density plateau, the jet inflates a cocoon whose shape in essentially spherical. During the following stages of evolution we must take into account two basic effects: the jet material that is thermalized at the jet terminal shock and forms the cocoon tends to escape along the direction along which the pressure gradient is steeper an then tends to form a transverse outflow. But the lateral flow must be fed by the material backflowing toward the center; if the jet exits the central region of higher density the jet head will increase its speed and the backflow will not feed the secondary flow and will stop to provide pressure support for the lateral expansion. In the simulation with the jet oriented along the major axis we see that the cocoon expands laterally due to the faster decrease in the external density in this direction. Moreover, the distribution of external gas causes a collimation of the outflow. This collimation is maintained also in the later stages of the evolution and produces an ordered outflow along the stratification minor axis. On the other hand, when the

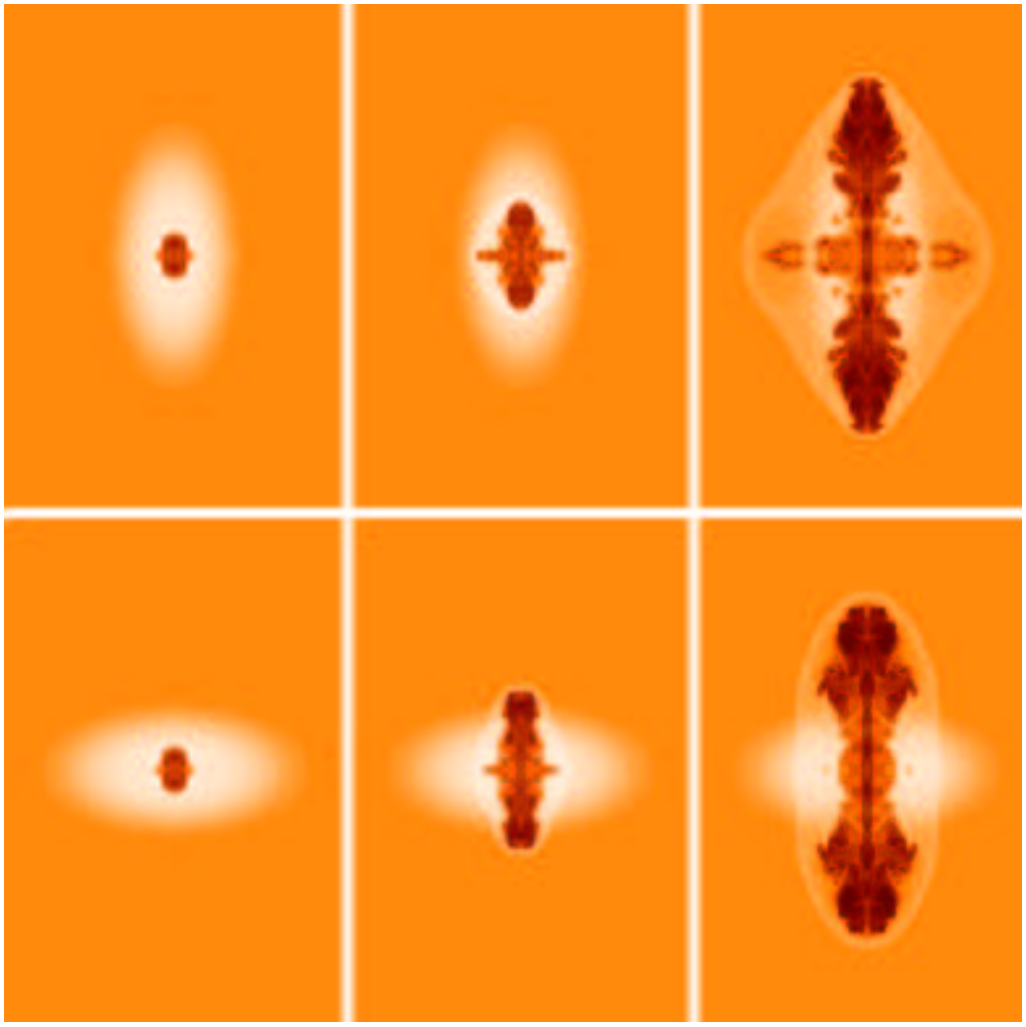

Fig. 6. Density maps of the 2D simulations showing the evolution of the cocoon in the stratified medium. The top panels refer to the case with the jet propagating along the major axis of the external distribution, while the lower panels to the case when the jet is oriented parallel to the minor axis.

jet is parallel to the minor axis, the lateral flow does not find a steep pressure gradient and then it is not highly accelerated. When the jet exits the central region the backflow stops to feed the outflow and no transverse flux is observed.

Our two-dimensional hydrodynamical simulations show clearly that an X-shaped structure naturally forms in an elliptically stratified ambient medium when the jet axis is oriented along the major axis of the stratification, while a classical double radio source forms when the jet propagates along the minor axis.

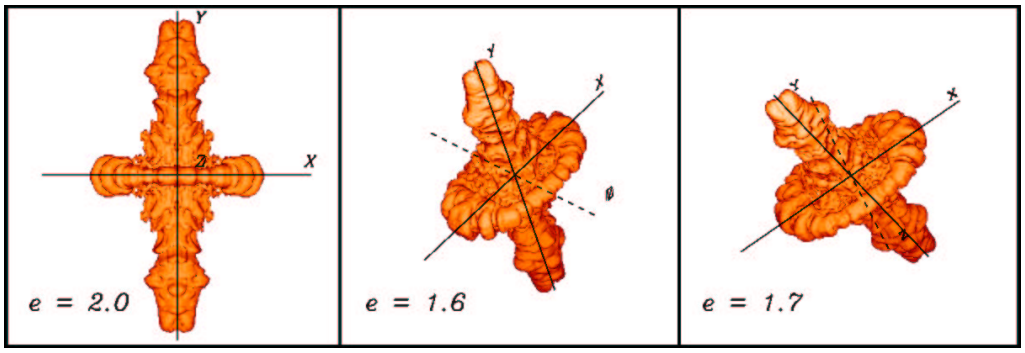

Fig. 7. Isodensity surfaces of the 3D simulated case of the propagation of a jet inside a triaxial density distribution. Each panel shows the cocoon as seen from different points of view. In each panel the ratio between the projected major and minor axis is shown.

3.3. 3D Simulation

Even if our 2D simulations show the importance of the external stratification in shaping the morphology of the lobes of extended radio sources, in particular in the case of X-shaped radio sources, these results have some severe limitations. First, due to the adopted cylindrical symmetry, the flow transverse to the jet axis shown in the first row of Fig. 5 is a circular equatorial outflow that suffers a strong dilution. Taking into account a triaxial stratification we can obtain a preferential direction along which the gas can escape, maintaining a stronger thrust with respect to the planar outflow that appears in the 2D simulations. In a 3D simulation then we can account for projection effects which can strongly modify the observed morphology of the lobes and can also lower the observed ellipticity of the host galaxy: one of the problem of the 2D simulations is that the assumed ellipticity of the stratification (correspondent to a ratio of 0.5 between the minor and the major axis) is the greatest observed in the sample of Capetti et al. (2002). We then performed a 3D simulation of a jet propagating along the major axis of a triaxial stratification. Along the three cartesian axes we assumed the same profiles shown in Fig. 5 and we took a ratio between the widths of the central plateau $r_x : r_y : r_z = 1 : 2 : 1.5$. Then we have a favored direction of expansion for the transverse flow along the x axis. The integration is performed in cartesian coordinates, the computational domain has a size $6r_x \times 6r_x \times 6r_x$ along the x, y, z axis respectively and has a resolution of $200 \times 200 \times 200$ grid points. We simulated only one eighth of the source and we adopted symmetry boundary conditions on the internal xy, yz and zx planes while free outflow boundary conditions are imposed on the outer planes. The jet has been put along the y axis ($x = 0, z = 0$) and we considered $M = 60$ and $\nu = 0.003$ as jet parameters. In Fig. 7 we show surfaces of constant density of the simulated cocoon as seen from different view angles. In the first panel on the left, that shows the cocoon as seen frontally, we see that thanks to the triaxial stratification, a more collimated outflow with respect to the 2D simulations is produced along the x axis along which we have imposed the steeper density gradient. From the other panels we can see that the expansion along the x direction is favored with respect to the z direction along which we have a less steep gradient. We can also see how the morphology of the transverse outflow can change as seen from other points of view and how the projected ratio between the major and the minor axis (reported in the panels as e) can increase because of projection effects thus giving a

lower observed ellipticity: we can then take the assumed maximum ellipticity as an upper limit.

4. Conclusions

We performed numerical simulations of the propagation of a supersonic underdense jet in an isothermal and stratified ambient medium. We considered different profiles for the external density distribution with different symmetries.

We have first performed 2D simulations in cylindrical geometry with a spherically stratified atmosphere. In agreement with the results of Reynolds et al. (2001) we found two distinct regimes of interaction between the cocoon formed by the jet and the ambient medium. In the first phase the cocoon is highly overpressured with respect to the external medium and drives a strong shock in it: the ambient material is then compressed in a thin and hot shell. In the second phase, the cocoon pressure lowers and tends to the external value: the shock becomes weak and the shell widens and cools down. We have found that these regimes of expansion correspond to very different X-ray morphologies. In the overpressured phase the images are dominated by a shell of enhanced emission surrounding the cocoon but no deficits of X-ray emission are observed. In the weakly overpressured phase the shell surrounds a deficit of emission coincident with the radio lobes.

Second we studied the effects of the anisotropies of the ambient medium on the morphology of the cocoon. We performed 2D simulations of a jet propagating in an atmosphere with elliptical symmetry and we found that if the jet is oriented along the major axis of the stratification, the transverse steeper pressure gradient can cause a lateral expansion of the cocoon at the same rate of the expansion along the major axis. This lateral expansion is collimated in an outflow that is similar to that observed in peculiar X-shaped radio sources (Capetti et al. 2002). If the jet propagates along the minor axis of the stratification a classical double radio source is formed. In order to better model this scenario we then performed a 3D simulation of a jet propagating inside a triaxial density distribution. We found results similar to the 2D simulations but we obtained a more collimated transverse outflow thanks to the fact that in 3D we were able to define a favored axis (not a plane as in cylindrical symmetry) for the propagation of the lateral flow. Taking into account projection effects we were also able to better model the morphology of X-shaped radio sources and to satisfy the constraints on the galaxy ellipticity.

References

Blanton E. L., Sarazin C. L., McNamara B. R., Wise M. W., 2001, ApJ 558, L15

Böhringer H., Nulsen P. E. J., Braun R., Fabian A. C., 1995, MNRAS 274, L67

Capetti A., Zamfir S., Rossi P., Bodo G., Zanni C., Massaglia S ., 2002, A&A 394, 39

Carilli C. L., Perley R. A., Harris D. E., 1994, MNRAS 270, 173

Clarke D. A., Harris D. E., Carilli, 1997, MNRAS 284, 981

Fabian A. C., Sanders J. S., Ettori S., Taylor G. B., Allen S. W . et al., 2000, MNRAS 318, L65

Krause M., 2002, astro–ph/0211448

Massaglia S., Bodo G., Ferrari A., 1996, A&A 307, 997

McNamara B. R., Wise M., Nulsen P. E. J., David L. P., Sarazin C . L., Bautz M. et al., 2000, ApJ 534, L135

Norman M. L., Smarr L., Winkler K. H. A., Smith M. D.,1982, A&A 113, 285

Nulsen P. E. J., David L. P., McNamara B. R., Jones C., Forman W . R., Wise M., 2002

Reynolds C. S., Heinz S., Begelman M. C., 2001, ApJ 549, L179

Reynolds C. S., Heinz S., Begelman M. C., 2002, MNRAS 332, 271

Rizza E., Loken C., Bliton M., Roettiger K., Burns J. O., 2000, AJ 119, 21

Smith D. A., Wilson A. S., Andrew S., Arnaud K. A., Terashima Y., Young A. J., 2002, ApJ 565, 195

Woodward P. R., Colella P., 1984, J. Comp. Phys. 54, 174